Structural Engineering and Mechanics, Vol. 5, No. 3 (1997) 257-268
DOI: http://dx.doi.org/10.12989/sem.1997.5.3.257

Elastic buckling of end-loaded, tapered, cantilevered beams with initial curvature

James F. Wilson †

Department of Civil and Environmental Engineering, Duke University, Durham, N.C. 27708-0287, U.S.A.

Daniel J. Strong ‡

North Carolina Department of Transportation, Raleigh, N.C. U.S.A.

Abstract. The elastic deflections and Euler buckling loads are investigated for a class of tapered and initially curved cantilevered beams subjected to loading at the tip. The beam's width increases linearly and its depth decreases linearly with the distance from the fixed end to the tip. Unloaded, the beam forms a circular arc perpendicular to the axis of bending. The beam's deflection responses, obtained by solving the differential equations in closed form, are presented in terms of four nondimensional system parameters: taper ratio κ, initial shape ratio Δ_0, end load ratio f, and load angle θ. Laboratory measurements of the Euler buckling loads for scale models of tapered, initially straight, corrugated beams compared favorably with those computed from the present analysis. The results are applicable to future designs of the end structures of highway guardrails, which can be designed to give the appropriate balance between the capacity to deflect a nearly head-on vehicle back to its right-of-way and the capacity to buckle sufficiently that penetration of the vehicle may be averted.

Key words: elastic buckling; Euler load; cantilevered beam; corrugated cross section; curved beam; guardrail; initial curvature; tapered beam; variable cross section.

1. Introduction

Historically, axially loaded tapered beams were discussed by Dinnik (1929, 1932), Timoshenko and Gere (1961), Ermopoulos (1986), Williams and Aston (1989), and Siginer (1992). These investigators computed Euler buckling loads for tapered beams of various cross sectional shapes (*I*-beams, box-beams, open web-beams, and beams of circular, square, and rectangular cross section), considering several types of end fixity. They expressed the taper along the beam's longitudinal coordinate x by choosing $I(x)$, the second moment of the cross sectional area with respect to the neutral axis in bending, as either an exponential function in x or a power law of x. For instance, Timoshenko and Gere (1961) used the latter form, or

$$I(x)=I\left(\frac{x}{a}\right)^m \tag{1}$$

in which I, a, and m are constants. This form is used herein to represent a tapered beam whose

† Professor
‡ Engineer

coordinate system, dimension a, and loading are shown in Fig. 1. Here, $m=2$ is used to model corrugations across the width, in which the width and depth tapers both vary linearly with the longitudinal coordinate x, as indicated in Fig. 2.

None of the historical analyses on the buckling of tapered beams has included the effects of initial beam curvature, which is the subject of the present study. An important application of tapered and initially curved beams subject to end loading is the terminal end structure of present-day highway guardrails. There are two main purposes of such structures: to buckle sufficiently so that penetration of the end structure into an impacting vehicle is avoided; and to have sufficient strength after buckling so that the impacting vehicle is deflected back into its traveling lane. Guardrail designers have reduced the guardrail buckling strength in two ways: by tapering (Sicking, *et al.* 1988); and by designing the second post from the end to release upon end impact, thereby effectively doubling the guardrail length and reducing its buckling strength by a factor of four (Bronstad, *et al.* 1986). What is new herein are the systematic studies of the interaction effects of taper, initial curvature, and angle of the end load on the deflection and buckling of cantilevered beams. These results may be applied to the future design of guardrail end structures that have the capacity to buckle while deflecting an incident vehicle in ways to improve the safety of passengers.

2. Mathematical model

Shown in Fig. 1 is the initially curved cantilevered beam of length L, lying in the horizontal or (x, y)-plane. The origin of the beam's (x, y) coordinate system is displaced by a from the tip of the beam. The tip load F is inclined at angle θ to the x-axis. The coordinate system is attached to the beam tip so that as the load is applied, the beam tip is always located at $(a, 0)$. The initial shape of the curve (for $F=0$) is defined by the circular arc in which the ordinate $y=y_0(x)$ and its curvature are, respectively

$$y_0(x)=\frac{d_0}{L^2}(L^2-(x-a-L)^2) \tag{2}$$

$$\frac{d^2y_0}{dx^2}=-2\frac{d_0}{L^2} \tag{3}$$

In these two Eqs. (2) and (3), d_0 is the initial, y-directed tip deflection relative to the fixed end, as shown in Fig. 1.

The geometric parameters for the linearly tapered, width-corrugated beam of this study are shown in Fig. 2. The corrugations of uniform thickness t are defined by the line segments of dimensions l_a, l_b, and l_c. The beam depth $w(x)$ is chosen as a linear function of the beam coordinate x, or

$$w(x)=(w_2-w_1)(x-a)/L+w_1 \tag{4}$$

where w_1 and w_2 are the depths at the tip and at the fixed end, respectively. For these corrugations, $I(x)$ is derived as

$$I(x)=4I_a(x)+2I_b(x)+2I_c(x) \tag{5}$$

where

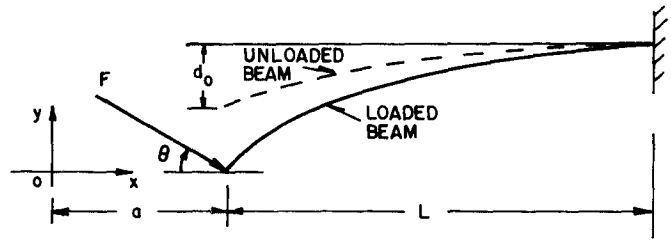

Fig. 1 Beam model in the *xy*-plane, showing dimensions, initial (or unloaded) beam shape, and the beam shape under tip load *F*.

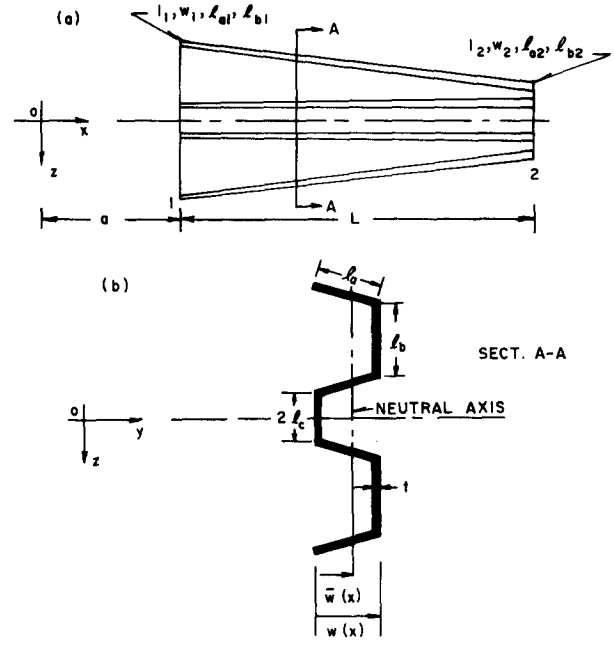

Fig. 2 Beam model showing: (a) linear taper in the *xz*-plane; and (b) typical cross section in the *yz*-plane with line segments defining the corrugations.

$$I_a(x)=\frac{l_a t w(x)^2}{12}+l_a t\left(\frac{w(x)}{2}-\bar{w}(x)\right)^2 \tag{6}$$

$$I_b(x)=\frac{l_b t^3}{12}+l_b t\left(w(x)-\bar{w}(x)-\frac{t}{2}\right)^2 \tag{7}$$

$$I_c(x)=\frac{l_c t^3}{12}+l_c t\left(\bar{w}(x)-\frac{t}{2}\right)^2 \tag{8}$$

and where the centroid of the cross sectional area with respect to the axis of bending is

$$\bar{w}(x)=\frac{l_a w(x)+l_b\left(w(x)-\frac{t}{2}\right)+\frac{1}{2}l_c t}{2l_a+l_b+l_c} \tag{9}$$

When Eqs. (4) and (6)-(9) are combined with Eq. (5), it is apparent that $I(x)$ has the form

$$I(x)=A_1x^2+A_2x+A_3 \tag{10}$$

in which A_1, A_2, and A_3 are constants involving products of the beam dimensions: l_a, l_b, l_c, w_1, w_2 and t. Here, l_a, l_b, and l_c are constant or linear functions of x. For thin-walled corrugations, Strong (1994) showed that $I(x)$ of Eq. (10) may be approximated by $A_1=I_1/a^2$, $A_2=A_3=0$, or

$$I(x)\approx I_1\left(\frac{x}{a}\right)^2 \tag{11}$$

where

$$a=\frac{L}{\kappa^{-1/2}-1};\ \kappa=I_1/I_2 \tag{12}$$

in which I_1 and I_2 are the values of $I(x)$ evaluated at the tip and at the fixed end, respectively. For instance, for a thin-walled corrugated section with $\kappa=I_1/I_2=0.25$, $I(x)$ computed from Eq. (11) has a maximum error of less than 0.02% when compared to the exact value computed from Eq. (10), based on Eqs. (4)-(9).

Consider now the equation governing the shape $y=y(x)$ of the beam with the tip load shown in Fig. 1. Assume classical beam theory, which then leads to the expression for the bending moment $M(x)$ as a function of the difference between the actual beam curvature and the initial curvature, or

$$M(x)=EI(x)\left(\frac{d^2y}{dx^2}-\frac{d^2y_0}{dx^2}\right) \tag{13}$$

where E is Young's modulus (Timoshenko and Gere 1961). In this class of problems, the bending moment is due to the tip load, or

$$M(x)=-(F\cos\theta)y-(F\sin\theta)(x-a) \tag{14}$$

When $I(x)$ of Eq. (11), the curvature of Eq. (3), and the moment of Eq. (14) are combined with Eq. (13), the equation governing the deflection of the beam becomes

$$EI_1\left(\frac{x}{a}\right)^2\frac{d^2y}{dx^2}+(F\cos\theta)y=-(F\sin\theta)(x-a)+EI_1\left(\frac{x}{a}\right)^2\frac{d^2y_0}{dx^2} \tag{15}$$

To solve Eq. (15), consider the following transformation and its derivative.

$$\frac{x}{a}=e^{\psi} \tag{16}$$

$$x^2\frac{d^2y}{dx^2}=\frac{d^2y}{d\psi^2}-\frac{dy}{d\psi} \tag{17}$$

With Eqs. (16), (17), and (3), Eq. (15) may be recast in terms of the independent variable ψ, or

$$\frac{d^2y}{d\psi^2}-\frac{dy}{d\psi}+\frac{Fa^2\cos\theta}{EI_1}y=-\frac{Fa^3\sin\theta}{EI_1}(e^{\psi}-1)-\frac{2a^2d_0}{L^2}e^{2\psi} \tag{18}$$

For a closed form solution to this governing equation, the methods of Moore (1962) are followed.

That is, the solution to the homogeneous equation is

$$y_h=\sqrt{e^{\psi}}(\bar{C}_1\sin\bar{\beta}\psi+\bar{C}_2\cos\bar{\beta}\psi) \tag{19}$$

where $\bar{C}_1$ and $\bar{C}_2$ are arbitrary constants and

$$\bar{\beta}=\sqrt{\frac{Fa^2\cos\theta}{EI_1}-\frac{1}{4}} \tag{20}$$

The homogeneous solution has the form

$$y_h=\bar{C}_1u_1(\psi)+\bar{C}_2u_2(\psi) \tag{21}$$

In these terms, the particular solution is written as

$$y=C_1(\psi)u_1(\psi)+C_2(\psi)u_2(\psi) \tag{22}$$

where the arbitrary constants $\bar{C}_1$ and $\bar{C}_2$ are now recast as c_1 and c_2 in the work that follows.

$$C_1(\psi)=-\int_0^{\psi}\frac{h(\psi)u_2(\psi)}{W[u_1(\psi),\ u_2(\psi)]}d\psi+c_1, \tag{23}$$

$$C_2(\psi)=\int_0^{\psi}\frac{h(\psi)u_1(\psi)}{W[u_1(\psi),\ u_2(\psi)]}d\psi+c_2, \tag{24}$$

$$h(\psi)=\frac{-Fa^2\sin\theta}{EI_1}(e^{\psi}-1)-\frac{2a^2d_0}{L^2}e^{2\psi} \tag{25}$$

The integrands of Eqs. (23) and (24) contain the Wronskian, defined as

$$W[u_1(\psi),\ u_2(\psi)]=\begin{vmatrix} u_1(\psi) & u_2(\psi) \\ u_1'(\psi) & u_2'(\psi)\end{vmatrix}=u_1(\psi)u_2'(\psi)-u_2(\psi)u_1'(\psi) \tag{26}$$

where $(')$ is the operator $d/d\psi$. The following two independent solutions to the homogeneous form of Eq. (18) are substituted into the Wronskian.

$$u_1(\psi)=\sqrt{e^{\psi}}\sin\bar{\beta}\psi \tag{27}$$

$$u_2(\psi)=\sqrt{e^{\psi}}\cos\bar{\beta}\psi \tag{28}$$

The Wronskian then becomes

$$W[u_1(\psi),\ u_2(\psi)]=-\bar{\beta}e^{\psi} \tag{29}$$

With this last result, Eqs. (23) and (24) become

$$C_1(\psi)=\int_0^{\psi}\frac{h(\psi)u_2(\psi)}{\bar{\beta}e^{\psi}}d\psi+c_1 \tag{30}$$

$$C_2(\psi)=-\int_0^{\psi}\frac{h(\psi)u_1(\psi)}{\bar{\beta}e^{\psi}}\,d\psi+c_2 \tag{31}$$

The solution is now cast in nondimensional form. The dependent and independent variables are

$$Y=y/L;\ \Psi=\frac{\psi}{ln\left(1+\frac{1}{A}\right)}=\frac{-2\psi}{ln(\kappa)};\ 0\le\Psi\le 1 \tag{32}$$

The taper ratio κ of Eq. (12) is expressed as

$$L/a=1/A=\kappa^{-1/2}-1 \tag{33}$$

The initial shape ratio is defined as

$$\Delta_0=d_0/L \tag{34}$$

The end load ratio is defined as

$$f=\frac{F}{\bar{F}_{cr}}=\frac{4}{\pi^2}\frac{FL^2}{EI_2} \tag{35}$$

In the latter equation, $\bar{F}_{cr}$ is the critical Euler buckling load for a uniform cantilevered beam in which $I(x)=I_2$, or

$$\bar{F}_{cr}=\frac{\pi^2}{4}\frac{EI_2}{L^2} \tag{36}$$

In these terms, the final solution to the governing differential equation becomes

$$\begin{aligned}Y(\psi)=&\left[\int_0^{\Psi}\frac{1}{\beta}\phi\kappa^{\Psi/4}h(\Psi)\cos(\beta\phi\Psi)\,d\Psi+c_1\right]\kappa^{-\Psi/4}\sin(\beta\phi\Psi)\\&+\left[-\int_0^{\Psi}\frac{1}{\beta}\phi\kappa^{\Psi/4}h(\Psi)\cos(\beta\phi\Psi)\,d\Psi+c_2\right]\kappa^{-\Psi/4}\cos(\beta\phi\Psi)\end{aligned} \tag{37}$$

where

$$h(\Psi)=-\frac{\pi^2}{4}fA^3\sin\theta(\kappa^{-\Psi/2}-1)-2\Delta_0A^2\kappa^{-\Psi} \tag{38}$$

$$\beta=\sqrt{\frac{\pi^2fA^2\cos\theta}{4\kappa}-\frac{1}{4}} \tag{39}$$

$$\phi=ln\left(1+\frac{1}{A}\right)=-\frac{1}{2}ln(\kappa) \tag{40}$$

The two arbitrary constants c_1 and c_2 of Eq. (37), the general solution to the second order differential Eq. (18), are computed by applying two geometric boundary conditions to Eq. (37), one at the tip and the other at the fixed end. (Note that the transverse shear and moment end conditions were incorporated in the initial second order model, Eq. (15) and that these loadings are satisfied at the ends as well). In the original coordinate system, the tip end condition

is $y(x)=0$ at $x=a$, and the fixed end condition is $dy/dx=0$ at $x=a+L$. In terms of the coordinate transformations defined by Eqs. (16) and (32), these respective end conditions are: $Y(\Psi)=0$ at $\Psi=0$ (or $Y(0)=0$); and $dY(\Psi)/d\Psi=0$ at $\Psi=1$ (or $Y'(1)=0$). When the tip end condition is applied to Eq. (37), then $c_2=0$; and when the fixed end condition is applied to the first derivative of Eq. (37), then the remaining constant is computed as

$$c_1=\int_0^1 \frac{1}{\beta}\phi\kappa^{\Psi/4}h(\Psi)\tan\alpha\ \sin(\beta\phi\Psi)\,d\Psi-\int_0^1 \frac{1}{\beta}\phi\kappa^{\Psi/4}h(\Psi)\cos(\beta\phi\Psi)\,d\Psi \tag{41}$$

where

$$\alpha=\tan^{-1}\left(\frac{1}{2\beta}\right)-\beta\phi \tag{42}$$

Consider the special case of the initially straight beam ($\Delta_0=0$) with a pure longitudinal load ($\theta=0$), for which the solution given by Eqs. (37)-(42) reduces to the following result.

$$Y(\Psi)=c_1\kappa^{-\Psi/2}\sin(\beta\phi\Psi) \tag{43}$$

in which $Y(0)=0$. Also in this special case,

$$Y'(\Psi)=c_1\left[\frac{\phi}{2}\kappa^{-\phi/4}\sin(\beta\phi\Psi)+\beta\phi\Psi^{-\phi/4}\cos(\beta\phi\Psi)\right] \tag{44}$$

which must satisfy the fixed end condition $Y'(1)=0$. This last condition leads to

$$\tan\beta\phi+2\beta=0 \tag{45}$$

The minimum nonzero root β of Eq. (45), when used with Eqs. (39) and (35), gives the critical ratio $f=f_{cr}$ and the Euler buckling load $F=F_{cr}$.

The results of the above analysis are summarized. The seven beam characteristics needed to compute the displacement curve and Euler buckling load for a linearly tapered beam with initial curvature are: the second moments of area at the ends, I_1 and I_2; the beam length and its initial offset, L and d_0; Young's modulus, E; and the tip load and its orientation, F and θ. These seven characteristics lead to four nondimensional system parameters: the taper ratio κ, Eq. (12); the initial shape ratio Δ_0, Eq. (34); the end load ratio f, Eq. (35); and the given load angle θ. With these parameters, A, $h(\Psi)$, β, ϕ, c_1, and α are computed from Eqs. (33) and (38)-(42), respectively. The solution for the beam's displacement is then computed from Eq. (37) in which $c_2=0$.

3. Numerical results

Consider first the special case described by Eqs. (43)-(45), the initially straight beam with a purely longitudinal load, and investigate the variation of the Euler buckling load with the taper ratio κ. Corresponding to the range of κ, which is 0 to 1, the range of the critical end load ratio $f=f_{cr}$ is $1/\pi^2$ to 1; and the range for the actual critical load F_{cr} is $E\,I_2/(4L^2)$ to $\pi^2\,E\,I_2/(4L^2)$. Typical results over the range of κ, as deduced from the smallest root β of Eq.

Table 1 Variation of buckling load ratio f_{cr} with the taper ratio κ, for $\Delta_0=\theta=0$

κ	β	$f_{cr}=\frac{4}{\pi^2}\frac{F_{cr}L^2}{EI_2}$
0.0	undefined	$1/\pi^2$
0.1	1.624	0.547
0.2	2.227	0.645
0.3	2.894	0.715
0.4	3.720	0.771
0.5	4.830	0.820
0.6	6.455	0.863
0.7	9.112	0.900
0.8	14.39	0.937
0.9	30.13	0.969
1.0	undefined	1.000

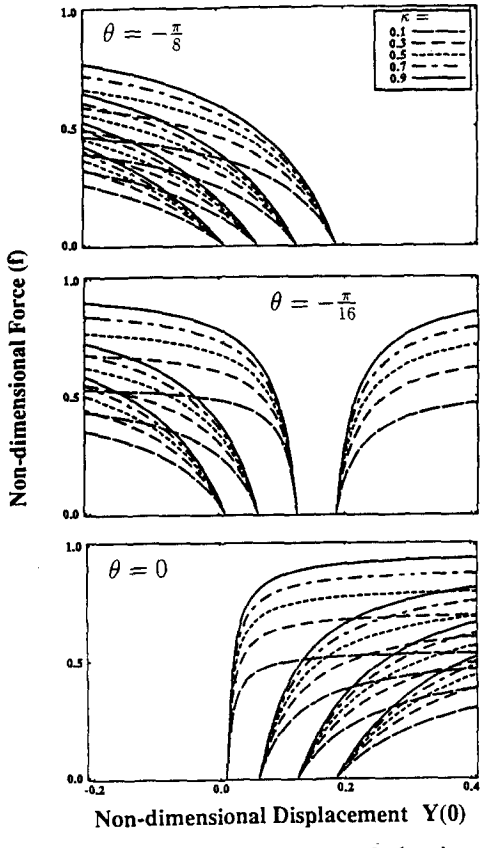

Fig. 3 End load-tip displacement behavior for $\theta=-\pi/8$, $-\pi/16$, and 0, for several values of the taper ratio κ. The the initial displacement ratios are $\Delta_0=0.01$, 0.0625, 0.125, and 0.1875, which are the points of intersection with the abscissa, left to right, respectively.

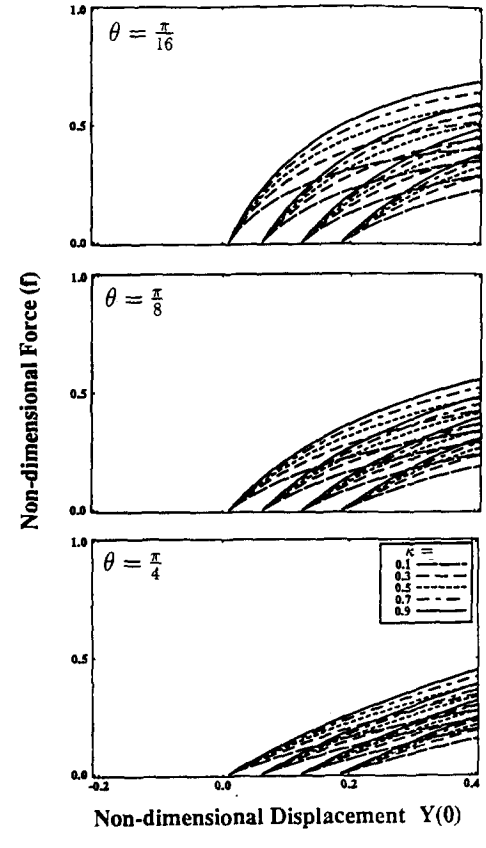

Fig. 4 End load-tip displacement behavior for $\theta=\pi/16$, $\pi/8$, and $\pi/4$ for several values of the taper ratio κ. The initial displacement ratios are $\Delta_0=0.01, 0.0625, 0.125$, and 0.1875, which are the points of intersection with the abscissa, left to right, respectively.

(45), together with Eqs. (39) and (35), are shown in Table 1. In practical cases, the taper is seen to reduce the buckling load by at most a factor of 2 ($\kappa \approx 0.1$) when compared to the buckling load for the uniform section ($\kappa=1$). The values of the Euler buckling load for this special case are upper bound values compared to the values computed for nonzero values of Δ_0 and (or) θ.

Using numerical integration, the exact solutions for the tip displacement $Y(0)=y(a)/L$ were computed for the following parameters: $\Delta_0=0.01$, 0.0625, 0.125, 0.1875; $\kappa=0.1$, 0.3, 0.5, 0.7, 0.9; and $\theta=-\pi/8$, $-\pi/16$, 0, $\pi/16$, $\pi/8$, and $\pi/4$. These results are shown in Figs. 3 and 4. In each of these figures, the four values of Δ_0 correspond to the four intersection points of the curves with the abscissa, for $f=0$. These results show a decrease in the load-carrying capacity of the beam as the taper ratio κ is decreased from 0.9 to 0.1, regardless of the values for Δ_0 and θ. Further, for a given κ and θ, the load-carrying capacity always decreases with increasing Δ_0.

In design applications involving guardrail end structures in which θ is expected to be greater than zero, then Fig. 4 applies. These results show that the effective load-carrying capacity may be reduced by a factor of two or more (in comparison to the uniform beam in which $\Delta_0=\theta=0$) if the following beam geometry is chosen: $\kappa \leq 0.7$ and $\Delta_0 \geq 0.0625$.

4. Experimental results and discussion

Experiments were designed and performed to measure Euler's buckling load for three different geometries of tapered, corrugated, steel beams that were initially as straight as manufacturing allowed ($\Delta_0 \approx 0$), where the load was purely longitudinal ($\theta=0$), or as near to this as possible experimentally. The purposes of the experiments were to observe local buckling, if any, in the vicinity of the corrugation bends and to determine how well the above analysis predicts Euler's buckling load for these shapes, keeping in mind that local buckling of the corrugations was not modeled in the analysis.

The geometric properties of the three types of experimental beams, all of the general type shown in Fig. 2, are summarized in Table 2. Each experimental beam had a linear taper in web depth as defined by Eq. (4), and a linear taper in the corrugated lengths l_a and l_b, given by

$$l_a=(l_{a2}-l_{a1})(x-a)/L+l_{a1} \tag{46}$$

$$l_b=(l_{b2}-l_{b1})(x-a)/L+l_{b1} \tag{47}$$

Here, the numerical subscripts (1,2) on these web dimensions refer to those at the wide and narrow end, respectively. In these specimens, l_c was constant and $I(x)$ had the form given by Eq. (11). For these steel specimens, Young's modulus was $E=207$ GN/m^2 and the tensile strength was 345 MN/m^2.

Each tapered, single beam was cold-formed from sheet steel, which was sandwiched between a series of flat plates and bent in a mechanical press to create the desired web shape. The experimental setup and a typical double beam specimen are shown schematically in Fig. 5. Each double beam specimen consisted of two tapered single beams of identical type, one of the three types defined in Table 2. The two single beams were overlapped and bolted together between steel bar stock at the narrow ends to form the clamped mid-section of the double-beam

Table 2 Geometric properties of the experimental specimens

Specimen property	Type 1	Type 2	Type 3
material thickness: t (cm)	0.0914	0.0914	0.0914
length: L (cm)	90.36	90.36	90.36
web depth, narrow end: (cm)	2.54	2.54	2.54
web depth, wide end: (cm)	2.54	2.06	1.43
narrow end: I_2(cm^4)	1.419	1.419	1.419
wide end: I_1(cm^4)	1.419	1.007	0.4745
$\kappa=I_1/I_2$	1.0	0.7097	0.3344

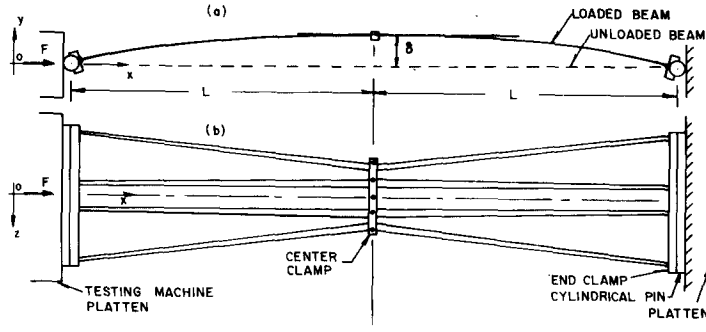

Fig. 5 Experimental setup of a double-beam specimen between plattens of the testing machine, showing: (a) beam displacement curve in the xy-plane and the measured midspan deflection δ; and (b) the linear taper in the xz-plane.

specimen. A cylindrical steel roller was affixed to each of the wide ends. This double-beam specimen was a pinned-pinned column of length $2L$, subjected to the longitudinal compressive load F, with a resulting central, lateral deflection δ in the xy-plane. It is observed that the half length of this double-beam specimen is identical to the model shown in Fig. 1: the single, tapered cantilevered beam of length L, with the tip load F at the wide end, where $\theta=d_0=0$ and $y(a)=\delta$. Note that $Y(0)=Ly(a)=L\delta$ by the transformation Eqs. (16) and (32).

A 2670 kN capacity Tinius-Olsen universal testing machine was used to apply the compressive end load, F, at the pinned ends. The full-scale load was set at 36 kN for which the measuring accuracy was ± 20 N. A dial gage with an 8 cm stroke and an accuracy of ± 0.002 cm was used to measure the lateral displacement δ at the center of the double beam. Each specimen was loaded slowly (the average test time was 30 minutes per specimen) and approximately 25 measurements of the compressive load and central lateral displacement were recorded simultaneously for each test. In all, nine experiments were performed: three tests for each of three identical specimens, Types 1, 2 and 3.

To determine the experimental buckling loads, a Southwell plot was generated for each of the nine specimens (Southwell 1912, Allen and Bulson 1980). The assumptions inherent in such plots are that the specimen is simply supported, and that the specimen has a small but finite initial curve due to imperfect manufacturing in which initial curve describing the imperfections is approximated by a half sine curve. For a typical set of experimental data (F, δ), the ratio F/δ vs. δ was plotted, and linear regression (excluding the first four points) was used to compute the slope formed by the remaining data. The inverse slope of this fitted curve was the experimental

Table 3 Euler's buckling loads, experimental and theoretical

Specimen Type	Measured buckling load (N)	Theoretical buckling load (N)
1A	8505	
1B	7455	
1C	8122	
Type 1, Average	8027	8496
2A	6699	
2B	6788	
2C	6681	
Type 2, Average	6723	7673
3A	5591	
3B	6410	
3C	6339	
Type 3 Average	6113	6227

Euler buckling load. The results of these experiments are given in Table 3, in which it is observed that the agreement between the measured Euler buckling loads and those computed from theory were all quite good. Based on the average of three specimens for each of the three geometries, the experimental loads were all somewhat lower than those predicted by theory: 5.52%, 12.4%, and 1.86% lower for specimen Types 1, 2, and 3, respectively.

There were three main reasons for the differences between the experimental and theoretical results. (1) Small initial specimen misalignment in the testing machine. Although every attempt was made to load the specimens in-line with the center of area with respect to the bending axis, the rapid displacement of the specimens at low loading indicated that there was sufficient initial offset to reduce the Euler buckling below that predicted by theory. The exception was specimen 1A, for which theory and experiment were essentially the same. (2) Manufacturing imperfections. As the maximum load was approached, the specimens exhibited local buckling of the unstiffened flanges (l_a), near midspan, in wave lengths of 7.6 cm, 10.2 cm, and 12.7 cm, which were precisely the lengths of the flat plates used in the mechanical press to form the specimens. (3) Effects of the bends. Due to bends that formed the corrugations, there was a reduction in effective area for the compressive stress in the unstiffened flanges (l_a) of the web (Kalyanaraman, *et al.* 1977 and DeWolf, *et al.* 1975). This could account for the closer agreement to the theory of the Type 3 specimens, which have the smallest unstiffened flanges of all three specimen types.

5. Conclusions

The closed-form load-displacement solutions for a class of tapered and initially curved cantilevered beams with tip loads showed reductions by factors of two to five in the effective elastic buckling loads, as compared to the buckling loads of their straight, uniform beam counterparts. Such reductions occurred for compressive loads oriented at $\theta > 0$ (Fig. 1), for taper ratios κ

and initial shape ratios Δ_0 spanning the realistic ranges as shown in Fig. 4.

The results of the present analysis, although based on thin-walled beams whose corrugated cross sections consisted of straight line segments, may be used also to determine the approximate buckling loads for end-loaded cantilevered beams with similar corrugations whose sharp line breaks are replaced by rounded corners, the geometry presently used for cantilevered-typeend structures of many highway guardrail designs. The present results are applicable to such designs that may overcome the shortcomings of the current ones, which are often so stiff in response to the end loads of errant vehicles that these end structures penetrate the vehicles, causing injury to the passengers. Future innovative end structure designs would make use of the results herein to achieve the proper balance between taper and initial curvature so that, in response to vehicle loading, terminal buckling and then vehicle deflection back to the travel lane would be accomplished with the least possible injury to passengers.

The experimental results for nine tapered, corrugated steel specimens of three different taper geometries and small initial curvature, all complemented this analysis. That is, for a given taper geometry, the measured buckling loads were about 2% to 12% lower than the predicted values, which indicates that the present analysis may be used with confidence for future designs, an example of which is the guardrail problem.

References

Allen, H.G. and Bulson, P.S. (1980), *Background to Buckling*, McGraw-Hill.

Bronstad, M.E., Meyer, J.B., Hatton, J.H. and Meczkowski, L.C. (1986), "Crash test evaluation of eccentric loader guardrail terminals", *Transportation Research Record 1065*, TRB, National Research Council.

DeWolf, J.T., Peokoz, T. and Winter, G. (1974), "Local and overall buckling of cold-formed members", *J. of Struct. Div., Proc. ASCE*, **100**(ST10).

Dinnik, A. (1929), "Design of columns of varying cross-section", *Trans. ASME*, **51**.

Dinnik, A. (1932), "Design of columns of varying cross-section", *Trans. ASME*, **54**.

Ermopoulos, J.C. (1986), "Buckling of tapered bars under stepped axial loads", *J. Struct. Engr.*, **112**(6).

Kalyanaraman, A.M., Pekoz, T. and Winter, G. (1977), "Unstiffened compression elements", *J. Struct. Div., Proc. ASCE*, **103**(ST9).

Moore, R.A. (1962), *Introduction to Differential Equations*, Allyn and Bacon, Inc, Boston.

Sicking, D.L., Qureshy, A.B., Bligh, R.P., Ross, H.E. Jr. and Buth, C.E. (1988) "Development of new guardrail end treatments", Texas Transportation Institute, Texas A & M Univ.

Siginer, A. (1992), "Buckling of columns of variable flexural rigidity", *J. Eng. Mech.*, **18**(3).

Southwell, R.V. (1912), "The strength of struts", *Engineering*, **94**.

Strong, D.J. (1994), "Tapered eccentric beam subjected to end loading", Master of Science Thesis, Dept. of Civil and Environmental Eng., Duke Univ., Durham, N.C.

Timoshenko, S.P. and Gere, J.M. (1961), *Theory of Elastic Stability*, McGraw-Hill.

Williams, F.W. and Aston, G. (1989), "Exact or lower bound tapered column buckling loads", *J. Struct. Eng.* **115**(5).